


# Impact of Optically Pumped Nonequilibrium Steady States on Luminescence Emission of Atomically Thin Semiconductor Excitons

Manuel Katzer<sup>1,\*†</sup>, Malte Selig<sup>1,\*</sup>, Dominik Christiansen,<sup>1</sup> Mariana V. Ballottin,<sup>2</sup>

Peter C. M. Christianen,<sup>2</sup> and Andreas Knorr<sup>1</sup>

<sup>1</sup>*Nichtlineare Optik und Quantenelektronik, Institut für Theoretische Physik, Technische Universität Berlin, 10623 Berlin, Germany*

<sup>2</sup>*High Field Magnet Laboratory (HFML-EMFL), Radboud University, Toernooiveld 7, Nijmegen 6525 ED, The Netherlands*

 (Received 10 January 2022; revised 1 June 2023; accepted 22 August 2023; published 2 October 2023)

The interplay of the nonequivalent corners in the Brillouin zone of transition metal dichalcogenides (TMDCs) has been investigated extensively. While experimental and theoretical works contributed to a detailed understanding of the relaxation of selective optical excitations and the related relaxation rates, only limited microscopic descriptions of stationary experiments are available so far. Here we present microscopic calculations for the nonequilibrium steady state properties of excitons during continuous wave pumping exemplary for monolayer MoSe<sub>2</sub>. We find sharp features in photoluminescence excitation spectra and degree of polarization which result from phonon assisted excitonic transitions dominating over exciton recombination and intervalley exchange coupling.

DOI: [10.1103/PhysRevLett.131.146201](https://doi.org/10.1103/PhysRevLett.131.146201)

**Introduction.**—Tightly bound excitons and strong exciton interactions in transition metal dichalcogenides have stimulated research over the past years [1–4]. Optically addressable excitons are located at the nonequivalent  $K/K'$  valleys in the hexagonal Brillouin zone, which can be excited with light of opposite circular polarization. The valley lifetime of selectively excited valley excitons is typically measured via pump probe experiments [1,5–9], time resolved luminescence experiments [10], or stationary luminescence [10–17]. Intervalley exchange coupling has been shown to mediate the relaxation between the valleys after optical excitation [18–20]. However, in the presence of energetically low lying momentum-indirect exciton states [21,22], the intervalley exchange coupling is suppressed [23], such that other spin relaxation mechanisms as Dyakonov-Perel [24,25] or Elliott-Yafet [9,25,26] gain importance. Such energetically low lying momentum-indirect states, such as  $(K, \Lambda)$  excitons in WSe<sub>2</sub> [22,27,28], are present in many TMDC materials. In contrast, MoSe<sub>2</sub> is considered as a candidate where momentum-indirect states are of minor importance and intervalley relaxation is governed through exchange coupling. While the ultrafast temporal behavior of optical excitations including the calculation of the different scatterings is well understood in MoSe<sub>2</sub> and also other materials, so far no theoretical studies have focused on the understanding of stationary experiments. As one candidate, stationary photoluminescence excitation (PLE) experiments are carried out to study the relaxation pathways of optical excitations. Here, several studies reported on the emergence of phonon replica which appear at excitation energies above the  $A$  exciton transition [29–31].

In this Letter we present a microscopic investigation of the interplay of exchange coupling and exciton-phonon interaction in monolayer MoSe<sub>2</sub> in stationary experiments under circular polarized continuous wave (cw) laser excitation. We take the detuning  $\Delta$  of the laser frequency located above the  $A$  exciton transition into account and explicitly evaluate its influence on the PLE and the degree of polarization (DoP) of the emitted light. Both the PLE and the DoP as a function of the detuning exhibit distinct features which can be traced back to phonon assisted excitonic transitions. Depending on the range of the detuning  $\Delta$ , we identify different microscopic processes which lead to the formation of specific spectral PLE features. (i) For increasing, but small detuning of few meV, the DoP decreases due to increasing off resonance. At larger detunings above 30 meV, phonon assisted transitions lead to an enhanced DoP, namely due to (ii) intravalley optical phonon emission processes, (iii) two  $\Lambda/M$  phonon emission processes, being assisted via virtual transitions at high energy excitonic valleys, and (iv) the stepwise relaxation due to two intravalley optical phonon emission processes. The calculated peaks in the PLE agree with recently reported measurements [29].

All in all, as the microscopic origin for these observations we identify the complex interplay of hot exciton formation via nonresonant cw excitation, intervalley exchange coupling, exciton-phonon scattering, and decay of excitons which contribute to the formation of a nonequilibrium steady state (NESS). The interplay of the individual contributions determining the PLE is illustrated

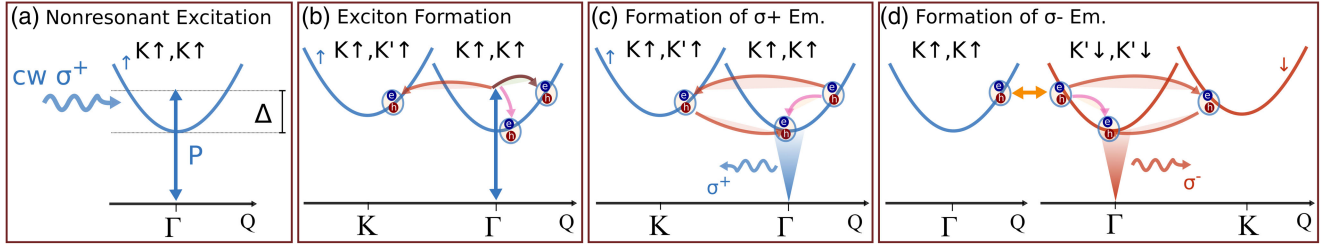


FIG. 1. Schematic illustration of the competing processes. (a) An excitonic coherence is nonresonantly pumped by the continuous wave light. (b) Exciton-phonon scattering mediates the formation of an incoherent occupation of exciton states. Here, optical  $\Gamma$  phonon scattering (pink arrow), acoustic  $\Gamma$  phonon scattering (brown arrow), and intervalley phonon scattering (red arrow) contribute. (c) Exciton-phonon scattering mediates the thermalization and population of states within the radiative cone (blue shaded area), leading to emission of  $\sigma_+$  polarized light ( $\sigma_+$  Em.). (d) For the population of the  $\sigma_-$  radiative cone (red shaded area), a stepwise process is required: (i) Intervalley exchange coupling (yellow arrow) has to generate  $\downarrow$  excitons and (ii) subsequent exciton phonon scattering populates the radiative cone, leading to emission of  $\sigma_-$  polarized light ( $\sigma_-$  Em.).

in detail in Fig. 1. First, cf. Fig. 1(a), the excitonic coherence  $P$  is excited with a  $\sigma_+$  polarized cw light pulse with a certain detuning  $\Delta$  from the  $A$  exciton transition in the  $(K\uparrow, K\uparrow)$  valley. The excitonic coherence decays via radiative decay [27,32], but more importantly through exciton-phonon interaction [27,33], cf. Fig. 1(b). The latter accounts for the formation of a hot incoherent exciton occupation in direct, as well as momentum-indirect  $(K\uparrow, K'\uparrow)$  exciton states. In the course of the formation of photoluminescence, two competing processes occur: the direct relaxation of excitons due to exciton-phonon scattering into the light cone of the pumped valley where  $\sigma_+$  polarized photons are emitted, cf. Fig. 1(c), or the subsequent exchange coupling and phonon mediated relaxation to the light cone of the unpumped valley where  $\sigma_-$  photons are emitted, cf. Fig. 1(d). The different efficiencies of the latter relaxation mechanisms determines the ratio of the intensity of  $\sigma_+$  and  $\sigma_-$  polarized light and thus the DoP. While all processes appear simultaneously, the resulting exciton distribution is in a NESS, which in general depends on the phonon temperature, the detuning of the exciting light field  $\Delta$ , as well as on the general lifetime of the excitons.

*Theory.*—To study the nonequilibrium steady states of excitons we start with the parametrization of the excitonic Hamiltonian [34] building on density-functional theory (DFT) calculations [35–37]. The Hamiltonian as well as all input parameters are summarized in Ref. [23] in Tables IV–IX. The next step is to calculate the equations of motion for the excitonic coherence  $P^{\xi_h \xi_e}(t)$  and incoherent exciton occupation  $N_{\mathbf{K}}^{\xi_h \xi_e}(t)$  with the compound valley spin of holes and electrons  $\xi_{h/e} = (i_{h/e}, s_{h/e})$  with valley  $i_{h/e}$  and spin  $s_{h/e}$  of the carriers and Fourier component of the center of mass motion  $\mathbf{K}$ . We take into consideration the exciton-light, exciton-phonon, and intervalley exchange coupling. From this we derive the Bloch equation for coupled excitonic coherence and the Boltzmann equation for the different incoherent exciton occupations [20,22,38], cf. Supplemental Material Sec. I [39]. While our microscopic evaluation reveals a radiative

lifetime of excitons in the order of hundreds of picoseconds [22], we include an additional decay  $\tau_{\text{dark}}^{-1}$  to our equations of motion, which can be attributed to dark recombination processes, e.g., exciton-exciton annihilation [54,55]. For our investigation we excite the excitonic coherence with a cw light field which is detuned from the excitonic energy by the detuning  $\Delta$ . We explicitly evaluate the steady state of the exciton occupation and calculate the polarization-resolved stationary photoluminescence with polarization  $\sigma = \sigma_+, \sigma_-$  [38,56], which reads

$$I^\sigma(\Delta) \propto \frac{2\pi}{\hbar} \sum_{\mathbf{K}, K_z, \xi} |d_{\mathbf{K}}^{\xi\sigma}|^2 N_{\mathbf{K}}^{\xi\xi}(\Delta, t \rightarrow \infty) \delta(\Delta E_{\mathbf{K}, K_z}^{\xi\sigma}), \quad (1)$$

with the dipole moment  $d_{\mathbf{K}}^{\xi\sigma}$ . The appearing delta function ensures the energy and momentum conservation during the radiative recombination. The emission depends on the amount of excitons  $N_{\mathbf{K}}^{\xi\xi}$  which are located in the radiative window (determined via the delta function),  $\Delta E_{\mathbf{K}, K_z}^{\xi\sigma} = E_{\mathbf{K}}^{\xi\xi} - \hbar\Omega_{\mathbf{K}, K_z}^\sigma$ , with the exciton dispersion  $E_{\mathbf{K}}^{\xi\xi}$  and the photon dispersion  $\hbar\Omega_{\mathbf{K}, K_z}^\sigma$  with the three-dimensional photon wave vector  $(\mathbf{K}, K_z)$ . Note that the stationary luminescence depends via the occupation  $N_{\mathbf{K}}^{\xi\xi}$  on the laser detuning via the exciton formation process, Sec. I in the Supplemental Material [39], and thus we write this dependence explicitly.

For the following, we numerically evaluate the exciton dynamics and the polarization-resolved photoluminescence for the material MoSe<sub>2</sub> on a quartz substrate. However, we have carefully checked that the described effects do not change qualitatively if we use different dielectric constants of the environment. If not stated differently, we use a lattice temperature of 7 K and an exciton lifetime  $\tau_{\text{dark}}$  of 5 ps. We take exciton-phonon coupling with the optical TO and the acoustic LA mode into account, cf. the detailed discussion in the Supplemental Material, Sec. IV [39].

*Photoluminescence excitation spectrum.*—Before studying the polarization resolved spectra, we start our

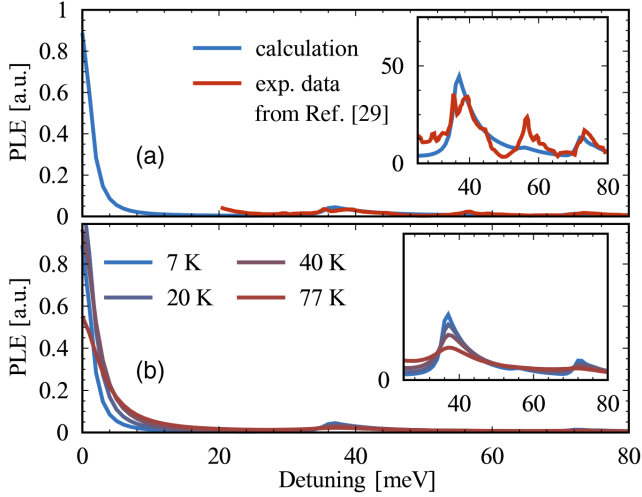


FIG. 2. Photoluminescence excitation spectrum at 7 K. (a) Comparison of the PLE for an exciton lifetime of 5 ps to the experimental data from Ref. [29]. The inset shows a magnification of the spectral region between 25 and 80 meV. (b) Spectra for an exciton lifetime of 5 ps at different lattice temperatures of 7, 20, 40, and 77 K.

investigation with the PLE spectrum in the nonequilibrium steady state as a function of the laser detuning  $\Delta$ :

$$\text{PLE}(\Delta) = [I^{\sigma_+}(\Delta) + I^{\sigma_-}(\Delta)]. \quad (2)$$

For long integration times in the experiment (more than nanoseconds), this measure is equivalent to the time integrated photoluminescence intensity.

The PLE measures how many radiatively active excitations are generated after excitation with a particular laser detuning  $\Delta$  from the excitonic  $A$  transition. In Fig. 2(a) we illustrate an exemplary PLE spectrum as a function of the laser detuning  $\Delta$ . First of all, we find a general decrease of the PLE due to the detuned excitation of the excitonic transition, cf. Supplemental Material Sec. I [39]. However, for detunings larger than 36 meV, we find a sharp increase of the PLE that can be traced back to efficient excitonic relaxation pathways, which are assisted by the emission of optical intravalley  $\Gamma$ TO at 36 meV [36] and a slight contribution of acoustic intervalley  $K$ LA phonons at 40 meV. Similarly, at energies above 72 meV, sharp features are observed due to the stepwise relaxation of excitons under the emission of two optical intravalley  $\Gamma$  phonons with exciton states in the  $(K\uparrow, K\uparrow)$  and  $(K'\downarrow, K'\downarrow)$  valleys as intermediate states. The intermediate spectral region is structureless. Here, incoherent excitons are formed through emission of one optical intravalley  $\Gamma$  phonon and the subsequent exciton relaxation is driven from acoustic intravalley  $\Gamma$ LA phonon scattering into the radiative cone. Since zone-edge acoustic phonons have a broad density of states, the corresponding feature in the PLE does not show any significant structure.

Additionally, we find a slight impact of two-phonon processes where two acoustic intervalley  $M$  phonons are

emitted with *virtual* exciton states at the  $(K\uparrow, \Lambda'\uparrow)$  and  $(K'\downarrow, \Lambda\downarrow)$  as intermediate states. We find a rather broad band of the two-phonon processes via virtual states, since different pathways contribute: We consider contributions from the intervalley  $MLA$  mode (19.7 meV) and the  $MTO$  mode (35.8 meV). Each combination of the latter phonons is involved in the  $\alpha, \alpha'$  summation in Eq. (S28), Supplemental Material Sec. II [39]. As a result, the two-phonon band begins at the energy of two intervalley  $MLA$  phonons (39.4 meV) and ends at the energy of two intervalley  $MTO$  phonons (71.6 meV). We find the most prominent contribution in the region of 50–60 meV, which originates from the two-phonon scattering involving one acoustic and one optical phonon. In this region, two-phonon processes are enhanced in comparison to the two-acoustic phonon region (32.8–39.4 meV) for combinatorial reasons.

Comparing our calculation with recent experimental results from Ref. [29] we find a relatively good agreement. The experiment exhibits a double peak at 36 and 40 meV which is reproduced by a broad resonance observed in theory. Our microscopic analysis reveals contributions from TO phonons at 36 meV and two LA phonon emission processes at 40 meV. The experiment further exhibits a strong peak at 54 meV. Despite the fact that our theory also predicts a resonance at 54 meV via combined TO-LA intervalley two-phonon processes, it is obvious that the experimentally observed magnitude is not reproduced. A possible reason is that we disregard virtual three-phonon transitions due to the computational complexity, which could contribute in this spectral region. Lastly, the experiment shows a resonance at 72 meV which is identified as the stepwise relaxation of two intravalley  $\Gamma$ TO phonons and is well captured by our calculation. See Sec. IV in the Supplemental Material [39] for a more detailed discussion.

Figure 2(b) illustrates the PLE spectrum at an exciton lifetime of  $\tau_{\text{dark}} = 5$  ps at selected lattice temperatures of  $T_{\text{lattice}} = 7\text{--}77$  K. We find that for increasing lattice temperature, two main effects can be observed. (i) The region at small detunings as well as all peaks which originate from phonon-induced excitonic transitions are significantly broadened. This can be traced back to the enhanced exciton-phonon scattering at elevated lattice temperatures, which results in a broadening of the absorption [22,27,40] and thus a broadening of the lines in the PLE. (ii) We find a general decrease of the PLE as a function of the lattice temperature: An increasing temperature results in hotter excitons. Consequently, less excitons occupy the bright state relevant for the photoluminescence, which reduces the PLE. However, we find that the ratio between phonon-induced peaks and PLE at  $\Delta = 0$  meV increases as a function of temperature due to more efficient exciton-optical phonon scattering at larger temperatures.

*Degree of polarization.*—The DoP of the emitted light defines the polarization contrast as a function of the laser detuning  $\Delta$ ; it is defined as

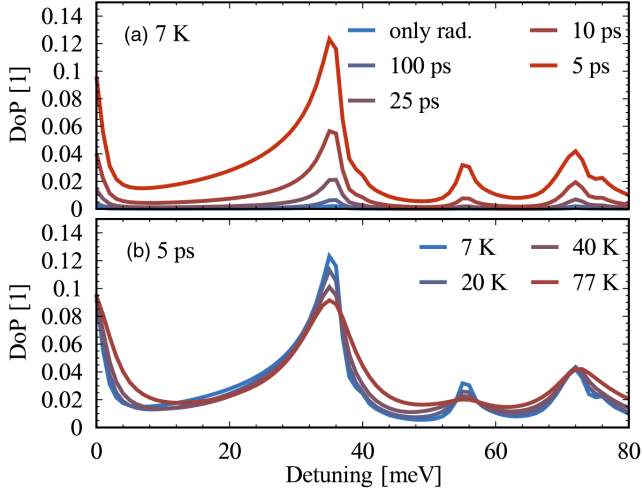


FIG. 3. Steady state degree of polarization in MoSe<sub>2</sub> as a function of detuning  $\Delta$  (a) at a lattice temperature  $T_{\text{lattice}} = 7$  K for different exciton lifetimes and (b) for a fixed exciton lifetime  $\tau_{\text{dark}} = 5$  ps at different lattice temperatures.

$$\text{DoP}(\Delta) = \frac{I^{\sigma_+}(\Delta) - I^{\sigma_-}(\Delta)}{I^{\sigma_+}(\Delta) + I^{\sigma_-}(\Delta)}. \quad (3)$$

Figure 3 illustrates the DoP in MoSe<sub>2</sub> as a function of laser detuning at a temperature of 7 K and an exciton lifetime of  $\tau_{\text{dark}} = 5$  ps. We find several features which originate from the complex interplay of exciton-phonon scattering, intervalley exchange coupling, and radiative recombination. (i) For increasing, but small detuning, we find that the DoP decreases, which originates from the simultaneously increasing exchange coupling element, and thus polarization mixing as a function of the center of mass momentum (and kinetic energy) occurs. (ii) At energies above 30 meV, we find sharp features in the DoP which can be traced back to phonon-induced transitions, which favor the relaxation into the light cone in the pumped valley, cf. Fig. 1(c), over the stepwise relaxation into the unpumped valley via exchange and subsequent phonon emission, cf. Fig. 1(d). We identify the same phonon transitions as for the discussion of the PLE, cf. Fig. 2(a).

In Fig. 3(a) we show the steady state DoP in MoSe<sub>2</sub> at  $T_{\text{lattice}} = 7$  K for different exciton lifetimes  $\tau_{\text{dark}}$ . We find that with decreasing lifetime, the DoP increases over the whole spectral range. This can be understood from the fact that the continuous pumping of excitons results in the formation of a NESS where the overall decay of the excitons significantly influences the steady state distribution. The inclusion of a short exciton lifetime in comparison to the intervalley exchange coupling prevents the excitons from coupling to the other valley relevant for  $\sigma_-$  emission resulting in a significant DoP. The observed order of magnitude ranges from less than 0.01 for only

incorporating the radiative decay to approximately 0.12 for an exciton lifetime of 5 ps.

Figure 3(b) illustrates the DoP as a function of laser detuning from the A exciton at an exciton lifetime of 5 ps but for varying lattice temperatures  $T_{\text{lattice}} = 7-77$  K. At all temperatures, we find a similar qualitative behavior of the DoP, including a decrease of the DoP at small detunings, and an increased DoP at certain energies which can be related to optical  $\Gamma$  phonon-induced transitions. Additionally, we find a broadening of all involved lines with increasing temperature, due to more intense exciton-phonon interaction.

*Effective excitonic temperatures.*—To determine the effective exciton temperatures of the NESS during cw pumping, we perform a Boltzmann fitting of the excitonic steady state distributions for different exciton lifetimes  $\tau_{\text{dark}}$  and laser detuning  $\Delta$ . The steady state distributions are discussed in the Supplemental Material, Sec. VI [39].

In Fig. 4 we show the effective temperature of the excitons at a lattice temperature of  $T_{\text{lattice}} = 7$  K for different exciton lifetimes  $\tau_{\text{dark}}$ . To obtain more insight, we also show the effective exciton temperature for pulsed excitation. The temperature is determined in the time window when the exciton occupation was already in quasiequilibrium due to exciton-phonon scattering but yet not decayed due to radiative and nonradiative recombination. First we find a general increase of the effective temperature as the lifetime decreases: excitons with short lifetimes do not have enough time to thermalize before they recombine (dark), and therefore the exciton distribution stays “hot.” If only radiative recombination is taken into account, we find that the effective temperature is only slightly larger compared to the pulsed excitation. We further find an overall increasing effective temperature as a function of detuning, due to more excess energy in the system. However, this increasing trend is interrupted at 30 and 36 meV and in the region above 60 meV, since for this excitation energy, the generated excitons can swiftly relax via the emission of optical phonons, leading to a cooling of the excitons effectively. The overall observation of a larger exciton temperature

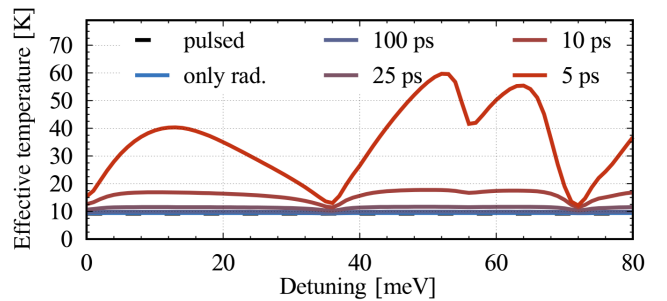


FIG. 4. Effective temperatures. Extracted effective exciton temperature at a lattice temperature of  $T_{\text{lattice}} = 7$  K in the steady state as a function of the laser detuning for different exciton lifetimes.

above the lattice temperature in cw experiments is consistent with a recent study of phonon sidebands in photoluminescence, where also an exciton temperature above the lattice temperature had to be assumed to match experimental and theoretical results [57].

*Conclusion.*—We presented microscopic calculations for the nonequilibrium steady state in monolayer MoSe<sub>2</sub> during continuous wave laser excitation. In agreement with available experimental data, we revealed that phonon mediated relaxation via emission of one optical  $\Gamma$  phonon or two optical and acoustic zone-edge phonons causes the appearance of pronounced phonon bands in the PLE. Furthermore, the DoP as a function of the laser detuning exhibits similar sidebands due to the domination of phonon assisted relaxation over intervalley exchange coupling. Our results further indicate that during cw pumping significant heating of excitons up to 40 K can be achieved.

We acknowledge great discussions with Hans Tonatzky (CNRS Toulouse) and Daniel Wigger (Wrocław University of Science and Technology). This work was funded by the Deutsche Forschungsgemeinschaft (DFG)—Project No. 182087777—SFB 951 (Project B12, M. S., D. C., M. K., A. K.). In addition, M. S. gratefully acknowledges funding from the Deutsche Forschungsgemeinschaft through Project No. 432266622 (SE 3098/1), and A. K. through Project No. 420760124 (KN 427/11-2). This work was supported by High Field Magnetic Laboratory-RU/NWO-I, member of the European Magnetic Field Laboratory (EMFL).

\*These authors contributed equally to this work.

<sup>†</sup>manuel.katzer@physik.tu-berlin.de

- [1] G. Wang, A. Chernikov, M. M. Glazov, T. F. Heinz, X. Marie, T. Amand, and B. Urbaszek, Colloquium: Excitons in atomically thin transition metal dichalcogenides, *Rev. Mod. Phys.* **90**, 021001 (2018).
- [2] D. Varsano, M. Palummo, E. Molinari, and M. Rontani, A monolayer transition-metal dichalcogenide as a topological excitonic insulator, *Nat. Nanotechnol.* **15**, 367 (2020).
- [3] C. Gies and A. Steinhoff, Atomically thin van der Waals semiconductors—A theoretical perspective, *Laser Photonics Rev.* **15**, 2000482 (2021).
- [4] S. Dong *et al.*, Direct measurement of key exciton properties: Energy, dynamics, and spatial distribution of the wave function, *Nat. Sci.* **1**, e10010 (2021).
- [5] Q. Wang, S. Ge, X. Li, J. Qiu, Y. Ji, J. Feng, and D. Sun, Valley carrier dynamics in monolayer molybdenum disulfide from helicity-resolved ultrafast pump-probe spectroscopy, *ACS Nano* **7**, 11087 (2013).
- [6] N. Kumar, J. He, D. He, Y. Wang, and H. Zhao, Valley and spin dynamics in MoSe<sub>2</sub> two-dimensional crystals, *Nanoscale* **6**, 12690 (2014).
- [7] S. Dal Conte *et al.*, Ultrafast valley relaxation dynamics in monolayer MoS<sub>2</sub> probed by nonequilibrium optical techniques, *Phys. Rev. B* **92**, 235425 (2015).
- [8] R. Schmidt, G. Berghäuser, R. Schneider, M. Selig, P. Tonndorf, E. Malić, A. Knorr, S. M. de Vasconcellos, and R. Bratschitsch, Ultrafast Coulomb-induced intervalley coupling in atomically thin WS<sub>2</sub>, *Nano Lett.* **16**, 2945 (2016).
- [9] Z. Wang *et al.*, Intravalley spin-flip relaxation dynamics in single-layer WS<sub>2</sub>, *Nano Lett.* **18**, 6882 (2018).
- [10] T. Yan, X. Qiao, P. Tan, and X. Zhang, Valley depolarization in monolayer WSe<sub>2</sub>, *Sci. Rep.* **5**, 15625 (2015).
- [11] G. Wang, E. Palleau, T. Amand, S. Tongay, X. Marie, and B. Urbaszek, Polarization and time-resolved photoluminescence spectroscopy of excitons in MoSe<sub>2</sub> monolayers, *Appl. Phys. Lett.* **106**, 112101 (2015).
- [12] D. H. Kim and D. Lim, The electrical and valley properties of monolayer MoSe<sub>2</sub>, *Curr. Appl. Phys.* **17**, 321 (2017).
- [13] T. Smoleński, M. Goryca, M. Koperski, C. Faugeras, T. Kazimierczuk, A. Bogucki, K. Nogajewski, P. Kossacki, and M. Potemski, Tuning Valley Polarization in a WSe<sub>2</sub> Monolayer with a Tiny Magnetic Field, *Phys. Rev. X* **6**, 021024 (2016).
- [14] H. Zeng, J. Dai, W. Yao, D. Xiao, and X. Cui, Valley polarization in MoS<sub>2</sub> monolayers by optical pumping, *Nat. Nanotechnol.* **7**, 490 (2012).
- [15] G. Kioseoglou, A. T. Hanbicki, M. Currie, A. L. Friedman, D. Gunlycke, and B. T. Jonker, Valley polarization and intervalley scattering in monolayer MoS<sub>2</sub>, *Appl. Phys. Lett.* **101**, 221907 (2012).
- [16] H. Tornatzky, A.-M. Kaulitz, and J. Maultzsch, Resonance Profiles of Valley Polarization in Single-Layer MoS<sub>2</sub> and MoSe<sub>2</sub>, *Phys. Rev. Lett.* **121**, 167401 (2018).
- [17] J. Jadczyk *et al.*, Room temperature multi-phonon upconversion photoluminescence in monolayer semiconductor WS<sub>2</sub>, *Nat. Commun.* **10**, 1 (2019).
- [18] T. Yu and M. W. Wu, Valley depolarization due to intervalley and intravalley electron-hole exchange interactions in monolayer MoS<sub>2</sub>, *Phys. Rev. B* **89**, 205303 (2014).
- [19] M. M. Glazov, T. Amand, X. Marie, D. Lagarde, L. Bouet, and B. Urbaszek, Exciton fine structure and spin decoherence in monolayers of transition metal dichalcogenides, *Phys. Rev. B* **89**, 201302(R) (2014).
- [20] M. Selig, F. Katsch, R. Schmidt, S. Michaelis de Vasconcellos, R. Bratschitsch, E. Malic, and A. Knorr, Ultrafast dynamics in monolayer transition metal dichalcogenides: Interplay of dark excitons, phonons, and intervalley exchange, *Phys. Rev. Res.* **1**, 022007(R) (2019).
- [21] D. Y. Qiu, T. Cao, and S. G. Louie, Nonanalyticity, Valley Quantum Phases, and Lightlike Exciton Dispersion in Monolayer Transition Metal Dichalcogenides: Theory and First-Principles Calculations, *Phys. Rev. Lett.* **115**, 176801 (2015).
- [22] M. Selig, G. Berghäuser, M. Richter, R. Bratschitsch, A. Knorr, and E. Malic, Dark and bright exciton formation, thermalization, and photoluminescence in monolayer transition metal dichalcogenides, *2D Mater.* **5**, 035017 (2018).
- [23] M. Selig, F. Katsch, S. Brem, Garnik F. Mkrtchian, E. Malic, and A. Knorr, Suppression of intervalley exchange coupling in the presence of momentum-dark states in transition metal dichalcogenides, *Phys. Rev. Res.* **2**, 023322 (2020).
- [24] L. Wang and M. Wu, Intrinsic electron spin relaxation due to the D'yakonov-Perel mechanism in monolayer MoS<sub>2</sub>, *Phys. Lett. A* **378**, 1336 (2014).

- [25] L. Wang and M. W. Wu, Electron spin relaxation due to D'yakonov-Perel' and Elliot-Yafet mechanisms in monolayer MoS<sub>2</sub>: Role of intravalley and intervalley processes, *Phys. Rev. B* **89**, 115302 (2014).
- [26] A. Molina-Sánchez, D. Sangalli, L. Wirtz, and A. Marini, *Ab initio* calculations of ultrashort carrier dynamics in two-dimensional materials: Valley depolarization in single-layer WSe<sub>2</sub>, *Nano Lett.* **17**, 4549 (2017).
- [27] M. Selig, G. Berghäuser, A. Raja, P. Nagler, C. Schüller, T. F. Heinz, T. Korn, A. Chernikov, E. Malic, and A. Knorr, Excitonic linewidth and coherence lifetime in monolayer transition metal dichalcogenides, *Nat. Commun.* **7**, 13279 (2016).
- [28] D. Christiansen *et al.*, Phonon Sidebands in Monolayer Transition Metal Dichalcogenides, *Phys. Rev. Lett.* **119**, 187402 (2017).
- [29] C. M. Chow *et al.*, Phonon-assisted oscillatory exciton dynamics in monolayer MoSe<sub>2</sub>, *npj 2D Mater. Appl.* **1**, 33 (2017).
- [30] C. M. Chow, H. Yu, A. M. Jones, J. Yan, D. G. Mandrus, T. Taniguchi, K. Watanabe, W. Yao, and X. Xu, Unusual exciton-phonon interactions at van der Waals engineered interfaces, *Nano Lett.* **17**, 1194 (2017).
- [31] S. Shree *et al.*, Observation of exciton-phonon coupling in MoSe<sub>2</sub> monolayers, *Phys. Rev. B* **98**, 035302 (2018).
- [32] H. Wang, C. Zhang, W. Chan, C. Manolatu, S. Tiwari, and F. Rana, Radiative lifetimes of excitons and trions in monolayers of the metal dichalcogenide MoS<sub>2</sub>, *Phys. Rev. B* **93**, 045407 (2016).
- [33] F. Lengers, T. Kuhn, and D. Reiter, Theory of the absorption line shape in monolayers of transition metal dichalcogenides, *Phys. Rev. B* **101**, 155304 (2020).
- [34] F. Katsch, M. Selig, A. Carmele, and A. Knorr, Theory of exciton-exciton interactions in monolayer transition metal dichalcogenides, *Phys. Status Solidi (b)* **255**, 1800185 (2018).
- [35] A. Kormanyos, G. Burkard, M. Gmitra, J. Fabian, V. Zólyomi, N. D. Drummond, and V. Fal'ko, *k p* theory for two-dimensional transition metal dichalcogenide semiconductors, *2D Mater.* **2**, 022001 (2015).
- [36] Z. Jin, X. Li, J. T. Mullen, and K. W. Kim, Intrinsic transport properties of electrons and holes in monolayer transition-metal dichalcogenides, *Phys. Rev. B* **90**, 045422 (2014).
- [37] M. L. Trolle, T. G. Pedersen, and V. Veniard, Model dielectric function for 2D semiconductors including substrate screening, *Sci. Rep.* **7**, 39844 (2017).
- [38] A. Thränhardt, S. Kuckenburg, A. Knorr, T. Meier, and S. W. Koch, Quantum theory of phonon-assisted exciton formation and luminescence in semiconductor quantum wells, *Phys. Rev. B* **62**, 2706 (2000).
- [39] See Supplemental Material at <http://link.aps.org/supplemental/10.1103/PhysRevLett.131.146201> for a detailed description of the theoretical model including a section on two-phonon processes and one on the details of the exciton-phonon interaction, as well as a variety of additional results, including the influence of the exciton lifetime, different excitation conditions, effective exciton temperatures, convergence times, snapshots of the dynamical formation of the NESS and details on the numerical implementation of the model, which includes Refs. [40–53].
- [40] Z. Khatibi, M. Feierabend, M. Selig, S. Brem, C. Linderälv, P. Erhart, and E. Malic, Impact of strain on the excitonic linewidth in transition metal dichalcogenides, *2D Mater.* **6**, 015015 (2018).
- [41] M. Katzer *et al.*, Exciton-phonon-scattering: A competition between bosonic and fermionic nature of bound electron-hole pairs, *Phys. Rev. B* **108**, L121102 (2023).
- [42] K. Kaasbjerg, K. S. Thygesen, and K. W. Jacobsen, Phonon-limited mobility in *n*-type single-layer MoS<sub>2</sub> from first principles, *Phys. Rev. B* **85**, 115317 (2012).
- [43] K. Kaasbjerg, K. S. Thygesen, and A.-P. Jauho, Acoustic phonon limited mobility in two-dimensional semiconductors: Deformation potential and piezoelectric scattering in monolayer MoS<sub>2</sub> from first principles, *Phys. Rev. B* **87**, 235312 (2013).
- [44] X. Li, J. T. Mullen, Z. Jin, K. M. Borysenko, M. B. Nardelli, and K. W. Kim, Intrinsic electrical transport properties of monolayer silicene and MoS<sub>2</sub> from first principles, *Phys. Rev. B* **87**, 115418 (2013).
- [45] G. Berghäuser and E. Malic, Analytical approach to excitonic properties of MoS<sub>2</sub>, *Phys. Rev. B* **89**, 125309 (2014).
- [46] N. S. Rytova, The screened potential of a point charge in a thin film, *Moscow Univ. Phys. Bull.* **3**, 18 (1967).
- [47] A. Knorr, S. Hughes, T. Stroucken, and S. Koch, Theory of ultrafast spatio-temporal dynamics in semiconductor heterostructures, *Chem. Phys.* **210**, 27 (1996).
- [48] M. Kira and S. Koch, Many-body correlations and excitonic effects in semiconductor spectroscopy, *Prog. Quantum Electron.* **30**, 155 (2006).
- [49] Y. Li, A. Chernikov, X. Zhang, A. Rigosi, H. M. Hill, A. M. van der Zande, D. A. Chenet, E.-M. Shih, J. Hone, and T. F. Heinz, Measurement of the optical dielectric function of monolayer transition-metal dichalcogenides: MoS<sub>2</sub>, MoSe<sub>2</sub>, WS<sub>2</sub>, and WSe<sub>2</sub>, *Phys. Rev. B* **90**, 205422 (2014).
- [50] F. A. Rasmussen and K. S. Thygesen, Computational 2D materials database: Electronic structure of transition-metal dichalcogenides and oxides, *J. Phys. Chem. C* **119**, 13169 (2015).
- [51] T. C. Berkelbach, M. S. Hybertsen, and D. R. Reichman, Theory of neutral and charged excitons in monolayer transition metal dichalcogenides, *Phys. Rev. B* **88**, 045318 (2013).
- [52] S. Meinecke, F. Köster, D. Christiansen, K. Lüdige, A. Knorr, and M. Selig, Data-driven forecasting of nonequilibrium solid-state dynamics, *Phys. Rev. B* **107**, 184306 (2023).
- [53] S. Meinecke, F. Köster, and M. Selig, Github repository "derrom," <https://github.com/stmeinecke/derrom>.
- [54] D. Erkensten *et al.*, Dark exciton-exciton annihilation in monolayer WSe<sub>2</sub>, *Phys. Rev. B* **104**, L241406 (2021).
- [55] A. Steinhoff, F. Jahnke, and M. Florian, Microscopic theory of exciton-exciton annihilation in two-dimensional semiconductors, *Phys. Rev. B* **104**, 155416 (2021).
- [56] M. Kira, F. Jahnke, W. Hoyer, and S. Koch, Quantum theory of spontaneous emission and coherent effects in semiconductor microstructures, *Prog. Quantum Electron.* **23**, 189 (1999).
- [57] S. Brem, A. Ekman, D. Christiansen, F. Katsch, M. Selig, C. Robert, X. Marie, B. Urbaszek, A. Knorr, and E. Malic, Phonon-assisted photoluminescence from indirect excitons in monolayers of transition-metal dichalcogenides, *Nano Lett.* **20**, 2849 (2020).